Original Article
OBESITY BIOLOGY AND INTEGRATED PHYSIOLOGY

Obesity

Incorporating Refractory Period in Mechanical Stimulation Mitigates Obesity-Induced Adipose Tissue Dysfunction in Adult Mice

Vihitaben S. Patel [1], *M. Ete Chan* [1], *Gabriel M. Pagnotti* [1], *Danielle M. Frechette* [1], *Janet Rubin* [2], *and Clinton T. Rubin* [1]

Objective: The aim of this study was to determine whether inclusion of a refractory period between bouts of low-magnitude mechanical stimulation (LMMS) can curb obesity-induced adipose tissue dysfunction and sequelae in adult mice.

Methods: A diet-induced obesity model that included a diet with 45% of kilocalories from fat was employed with intention to treat. C57BL/6J mice were weight matched into four groups: low-fat diet (LFD, $n = 8$), high-fat diet (HFD, $n = 8$), HFD with one bout of 30-minute LMMS (HFDv, $n = 9$), and HFD with two bouts of 15-minute LMMS with a 5-hour separation (refractory period, RHFDv, $n = 9$). Two weeks of diet was followed by 6 weeks of diet plus LMMS.

Results: HFD and HFDv mice continued gaining body weight and visceral adiposity throughout the experiment, which was mitigated in RHFDv mice. Compared with LFD mice, HFD and HFDv mice had increased rates of adipocyte hypertrophy, increased immune cell infiltration (B cells, T cells, and macrophages) into adipose tissue, increased adipose tissue inflammation (tumor necrosis factor alpha gene expression), and a decreased proportion of mesenchymal stem cells in adipose tissue, all of which were rescued in RHFDv mice. Glucose intolerance and insulin resistance were elevated in HFD and HFDv mice, but not in RHFDv mice, as compared with LFD mice.

Conclusions: Incorporating a 5-hour refractory period between bouts of LMMS attenuates obesity-induced adipose tissue dysfunction and improves glucose metabolism.

Obesity (2017) **00**, 00–00. doi:10.1002/oby.21958

Introduction

Obesity continues to grow at an alarming rate in the United States, doubling in the past 30 years, with more than one-third of the adult population suffering from this condition (1). This is a major health concern because obesity increases susceptibility to a range of life-threatening sequelae, such as cardiovascular diseases, hypertension, cancer, and type 2 diabetes (T2D). These obesity-associated comorbidities not only reduce quality of life but also pose a significant economic burden, costing approximately $147 billion per year in the United States (2). Thus, it is crucial to develop a cost-effective and widely accessible treatment for obesity.

One of the primary sites affected by obesity is adipose tissue, a metabolically active tissue that functions as a storage compartment for excess energy (3). Overconsumption during obesity leads to excessive lipid storage in adipocytes, resulting in adipocyte hypertrophy, which can induce fat necrosis and release of proinflammatory cytokines (4). Adipose tissue dysfunction and the chronic inflammatory state associated with obesity have been shown to contribute to insulin resistance and glucose intolerance, the underlying causes for T2D (5). There is accumulating evidence that exercise, a primary treatment modality for obesity, plays a role in strengthening the immune system and reducing adipose tissue inflammation (6,7). Although treatment with exercise avoids the inherent risks of pharmaceuticals, the demands of daily physical exertion are not easily achieved by those with morbid obesity (8).

In contrast to strenuous exercise, low-magnitude mechanical stimulation (LMMS) delivered via low-intensity vibration (LIV) has been shown to suppress adipogenesis and adiposity, not by increasing metabolism of existing tissue, but by biasing lineage selection in mesenchymal stem cell (MSC) differentiation (9-11). In addition to playing a principal role in adipogenesis, MSCs have been shown to exhibit

[1] Department of Biomedical Engineering, Stony Brook University, Stony Brook, New York, USA. Correspondence: Clinton T. Rubin (clinton.rubin@stonybrook.edu) [2] Department of Medicine, University of North Carolina at Chapel Hill, Chapel Hill, North Carolina, USA.

Funding agencies: This work was supported by the National Institutes of Health through the National Institute of Arthritis and Musculoskeletal and Skin Diseases (AR-43498) and the National Institute of Biomedical Imaging and Bioengineering (EB-14351).

Disclosure: CTR has authored patents related to the mechanical regulation of metabolic diseases and is a founder of Marodyne Medical. The other authors declared no conflict of interest.

Received: 6 April 2017; **Accepted:** 19 July 2017; **Published online 00 Month 2017. doi:10.1002/oby.21958**

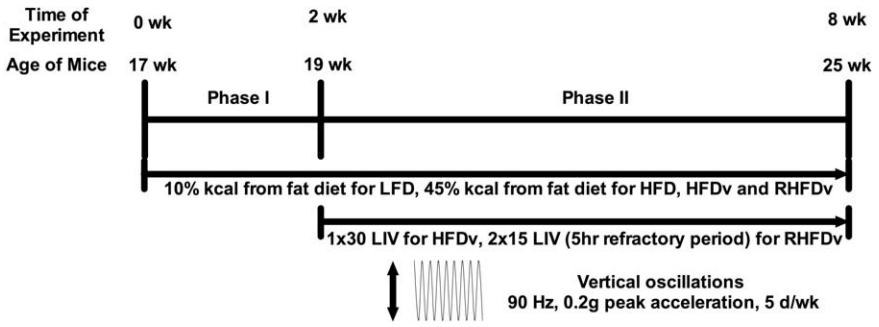

Figure 1 Experimental timeline consisting of two phases. During phase one (initial 2 weeks), while LFD mice were fed 10% of their kilocalories from fat, HFD, HFDv, and RHFDv mice were fed 45% of their kilocalories from fat to induce the obesity phenotype. During phase two (6 weeks following phase one), HFDv and RHFDv mice underwent LIV stimulation (vertical oscillations, 90Hz, 0.2*g* peak acceleration, 5 d/wk) for one bout of 30 minutes per day (1×30) and two bouts of 15 minutes per day with a 5-hour refractory period (2×15), respectively. All mice were euthanized at 8 weeks following the start of experiment at the age of 25 weeks.

an immunosuppressive effect by regulating proliferation of lymphocytes both *in vitro* and *in vivo* and by triggering macrophages to produce anti-inflammatory cytokines, such as interleukin 10 (12,13). Interestingly, LIV has also been shown to play a role in altering immune responses by increasing the bone marrow B cell population that is depleted by diet-induced obesity (14). Thus, targeting MSCs and the immune system simultaneously via LIV could potentially mitigate the pernicious consequences of obesity. The challenge of using LMMS in adults to treat obesity is that the sensitivity to mechanical stimulation may have already disappeared (15). Published work on LMMS has shown that the younger the subject, whether mouse or human, the more effective the signal (16), a finding that suggests an age-dependent decline in cell mechanosensitivity (17).

One potential solution to address reduced mechanosensitivity in adults could be the inclusion of a refractory period between loading bouts (18). At the cellular level, inclusion of a 3-hour refractory period between LMMS bouts has been shown to enhance adipogenesis suppression (19,20). In a murine model, the incorporation of a 5-hour refractory period between LMMS bouts led to an increased MSC population in the bone marrow (21). Hence, in this experiment, we aimed to determine whether this effect could be extended at the metabolic level *in vivo*. We hypothesized that inclusion of a 5-hour refractory period between bouts of LIV could mitigate obesity-induced adipose tissue dysfunction, and subsequently T2D, in adult mice.

Methods

Diet-induced obesity model and mechanical stimulation

All animal protocols were reviewed and approved by the Stony Brook University Institutional Animal Care and Use Committee. Starting from 17 weeks old, 34 male C57BL/6J mice (The Jackson Laboratory, Bar Harbor, Maine) were weight matched into four groups: low-fat diet (LFD, $n = 8$), high-fat diet (HFD, $n = 8$), HFD with one 30-minute bout (1×30) of mechanical stimulation (HFDv, $n = 9$), and HFD with two 15-minute bouts (2×15) of mechanical stimulation with a 5-hour refractory period between bouts (RHFDv, $n = 9$). All mice were housed singly and had ad libitum access to food and water. The intention-to-treat model consisted of two phases (Figure 1). During both phases, LFD mice were fed a diet in which 10% of the kilocalories came from fat (58Y2 VanHeek series; TestDiet, St. Louis, Missouri), while HFD, HFDv, and RHFDv mice were fed a diet in which 45% of the kilocalories came from fat (58V8 VanHeek series; TestDiet). Phase one (2 weeks) consisted of diet-only treatment to induce the obesity phenotype. During phase two (6 weeks following phase one), HFDv and RHFDv mice were mechanically stimulated via LIV protocol (0.2*g* peak acceleration [$1.0g = 9.81\,m/s^2$], 90 Hz, 5 d/wk) for 1×30 and 2×15, respectively, using a vertically oscillating platform (Marodyne LiV; Marodyne Medical, Tampa, Florida). During each LIV delivery, the groups that were not being stimulated were sham-handled by placing them on an inactive vibration platform. Body weight and calorie intake were measured weekly. At the end of the experiment, animals were euthanized via CO_2 inhalation followed by cervical dislocation. The gonadal fat pad weight for each animal was measured at euthanasia.

Quantification of abdominal adiposity by microcomputed tomography

Abdominal adiposity was quantified *in vivo* using microcomputed tomography (vivaCT 40; Scanco Medical, Inc., Wayne, Pennsylvania). Mice were scanned at two time points: at the end of phase one and at the end of phase two. All scans were performed at 45 kV(p), 133 μA, 125 projections per 180°, and 76 μm resolution (22). During scans, mice were maintained under anesthesia (2% isoflurane inhalation) and placed in a custom-designed foam holder to prevent body movements. Total adipose tissue (TAT) was measured across the abdominal region between the L1 and L5 lumbar vertebrae. TAT was further segregated into subcutaneous adipose tissue (SAT) and visceral adipose tissue (VAT) by using an automated script (23).

Adipocyte area measurement

Half of the left gonadal fat pad for each mouse was embedded in paraffin, sectioned (10 μm), and stained with standard hematoxylin

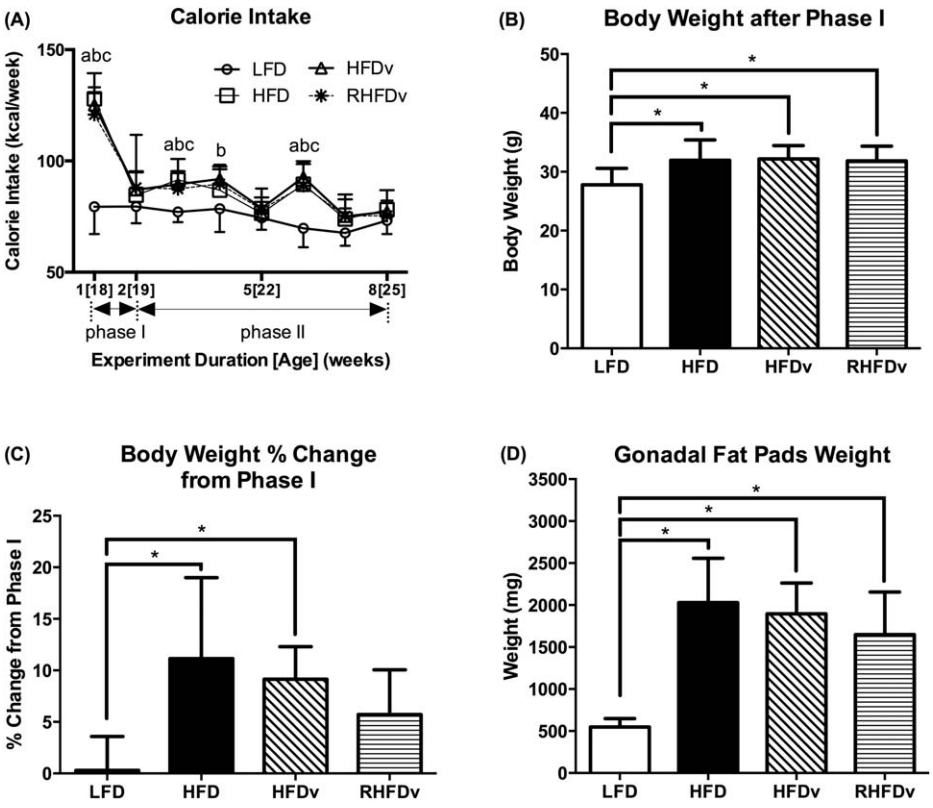

Figure 2 Diet-induced obesity model. (**A**) Mice on high-fat diet (HFD, HFDv, and RHFDv groups) had an increased calorie intake compared with mice fed a low-fat diet throughout the experiment. (**B**) Increased body weight in HFD, HFDv, and RHFDv mice at the end of phase one (2 weeks on high-fat diet), as compared with LFD mice, prior to LIV treatment ($P < 0.05$). (**C**) Percent change in body weight of each animal during phase two, after 6 weeks of LIV treatment. There was a continued increase in body weight in HFD and HFDv mice ($P < 0.05$) and a slowed progression in RHFDv mice ($P =$ not significant), as compared with LFD mice. (**D**) Increased gonadal fat pad weight in HFD, HFDv, and RHFDv mice at the end of experiment ($P < 0.05$). All data sets were normally distributed, and data are presented as mean ± SD. $^{a}P < 0.05$, LFD versus HFD. $^{b}P < 0.05$, LFD versus HFDv. $^{c}P < 0.05$, LFD versus RHFDv. $^{*}P < 0.05$.

and eosin. Three nonconsecutive sections from each animal were imaged at three randomly selected areas (a total of nine areas per animal) at a magnification of 400 × and were evaluated using ImageJ (National Institutes of Health, Bethesda, Maryland) (24). The boundary of each adipocyte was manually traced using the "Freehand selections" tool, and the area of each adipocyte was measured using the "Measure" tool. All imaging evaluations were performed blinded to the experimental group.

Flow cytometry analysis

Right gonadal fat pads were dissociated by immersing in collagenase type 2 (Worthington Biochemical Corp., Lakewood, New Jersey) and by manually straining them through a 70-μm strainer. Red blood cells were lysed using 1 × Pharmlyse (BD Biosciences, San Jose, California). A single-cell suspension containing 2×10^6 cells was prepared from each animal to identify MSCs (Sca-1[PE]$^+$, CD90.2[APC]$^+$, C-kit[PerCP/Cy5.5]$^+$, CD105[PE/Cy7]$^+$, and CD44[Pacific Blue]$^+$), B cells (B220[PerCP/Cy5.5]$^+$), T cells (CD4[PE]$^+$), and macrophages (F4/80[FITC]$^+$) via flow cytometry (FACSAria, FACSCalibur; BD Biosciences) (9,25-28). Distinct spectra of emission wavelengths were chosen for each fluorochrome conjugate to avoid overlaps in cell populations.

RNA extraction and real-time reverse transcription-polymerase chain reactions

Half of the left gonadal fat pad from each mouse was preserved in RNA-*later* (Life Technologies, Grand Island, New York). Total RNA was extracted using RNeasy lipid tissue mini kit (Qiagen Sciences, Inc., Germantown, Maryland). The amount of RNA was measured by a NanoDrop spectrophotometer (NanoDrop Technologies, LLC, Wilimington, Delaware). Each RNA sample was diluted to 10 ng/μl. The diluted RNA samples were converted to complementary DNA by using a high-capacity cDNA reverse transcription kit (Life Technologies). Real-time reverse transcription-polymerase chain reactions were produced using TaqMan gene expression assays (Life Technologies) for tumor necrosis factor alpha (TNF-α, Mm00443258_m1) and insulin receptor substrate 1 (IRS1; Mm01278327_m1). All expression levels were measured with respect to LFD mice and were normalized to mouse 18S ribosomal RNA (Mm03928990_g1; Life Technologies) (29).

Plasma insulin measurement and glucose tolerance test

Plasma insulin measurements and glucose tolerance tests were performed at the end of phase two. After overnight fasting, blood was

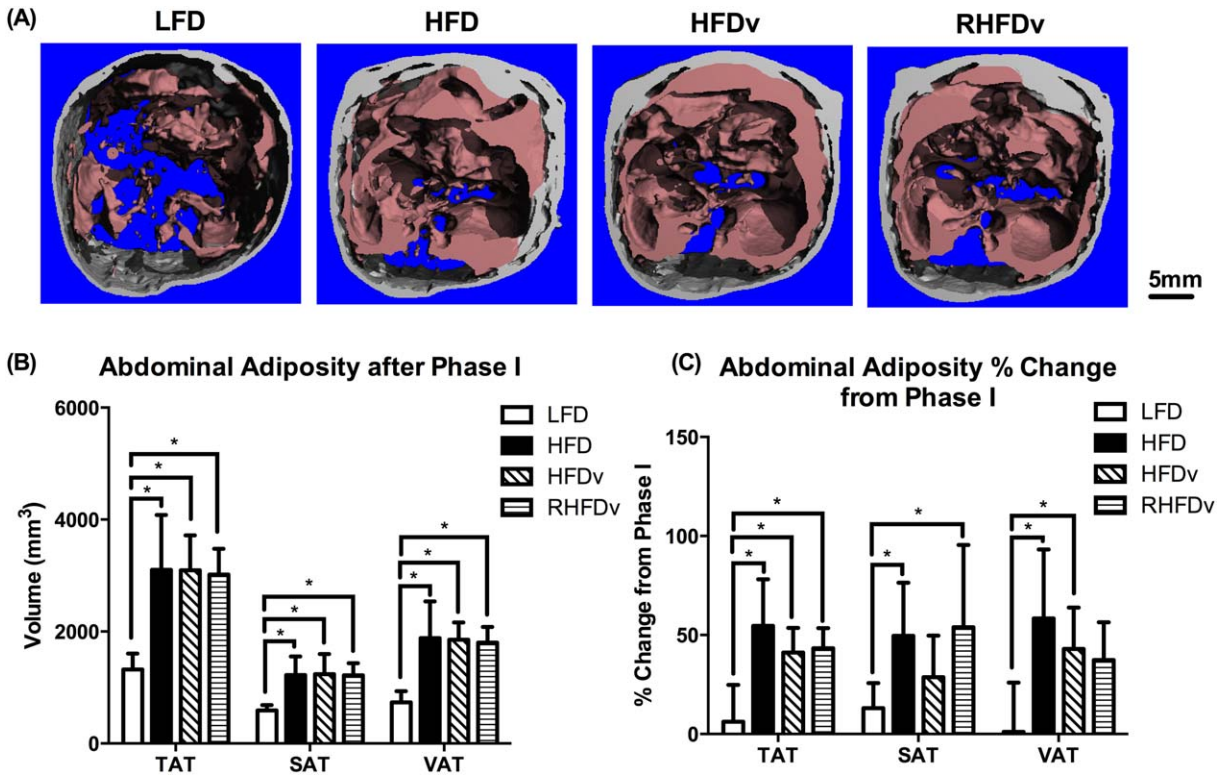

Figure 3 Abdominal adiposity. (**A**) Representative microcomputed tomography sections of transverse abdominal region to demonstrate the distribution of SAT (gray) and VAT (pink) in LFD, HFD, HFDv, and RHFDv mice (from left to right) at the end of phase two. (**B**) Increased TAT, SAT, and VAT in all high-fat diet groups at the end of phase one, as compared with the LFD group, before LIV treatment ($P < 0.05$). (**C**) Percent change in TAT, SAT, and VAT of each animal from the end of phase one. A continued increase in TAT in HFD, HFDv, and RHFDv mice ($P < 0.05$) is shown. Whereas the increase in TAT was a result of increased VAT for HFD and HFDv mice, RHFDv promoted SAT gain and mitigated VAT gain. All data sets were normally distributed, and data are presented as mean ± SD. *$P < 0.05$.

collected via tail-tip transection, and plasma was isolated by centrifugation. Fasting plasma insulin was measured by using a mouse insulin ELISA kit, with rat insulin as a standard (EMD Millipore, St. Charles, Missouri). Fasting blood glucose was measured by using the ACCU-CHEK Aviva system (Roche Diagnostics, Basel, Switzerland). Mice were then injected intraperitoneally with a 20% dextrose solution in sterile saline (Sigma-Aldrich, St Louis, Missouri) at the dosage of 0.75 g of dextrose per each kilogram of body weight. Blood glucose was measured at 15, 30, 45, 60, 90, and 120 minutes after the injection. Glucose intolerance was quantified by calculating the area under the curve in blood glucose versus time graph using the trapezoidal method.

Statistical analysis

Normality was accessed via the Shapiro-Wilk test, with $\alpha = 0.05$. Normally distributed data sets were analyzed using one-way analysis of variance (ANOVA) (Tukey's post hoc test) and presented as mean ± SD, whereas nonnormally distributed data sets were analyzed by using the Kruskal-Wallis test (Dunn's post hoc test) and presented as box plot data (median, interquartile range, minimum and maximum) (GraphPad Prism; GraphPad Software, Inc., San Diego, California). Correlations were determined by calculating the Pearson correlation coefficient. $P < 0.05$ was considered significant. Outliers were determined via Grubbs' test, with $\alpha = 0.01$. One of the RHFDv animal's data were excluded from all data analyses because of the animal's sickness toward the end of the experiment.

Results

Increased calorie intake with high-fat diet

All mice on a high-fat diet had a higher calorie intake than the LFD group throughout the experiment. The largest difference in calorie intake was seen during the first week, when the HFD, HFDv, and RHFDv groups had 61%, 58%, and 52% higher calorie intakes, respectively, than the LFD group ($P < 0.05$, Figure 2A).

Increased body weight and gonadal fat weight with high-fat diet

All animals on high-fat diet were 15% heavier than those on low-fat diet at the end of phase one ($P < 0.05$, Figure 2B). During phase two, while LFD mice maintained their body weight, the body weight of HFD and HFDv mice increased by 11% and 9%, respectively ($P < 0.05$, compared with LFD mice). RHFDv mice showed slowed progression in weight gain, with only a 5% increase in body weight during phase two (P = not significant, compared with LFD mice, Figure 2C). Gonadal fat pad weight increased in HFD (2,028 ± 528 mg), HFDv (1,893 ± 368 mg), and RHFDv (1,648 ± 507 mg) mice, as compared with LFD mice (549 ± 99 mg) ($P < 0.05$, Figure 2D).

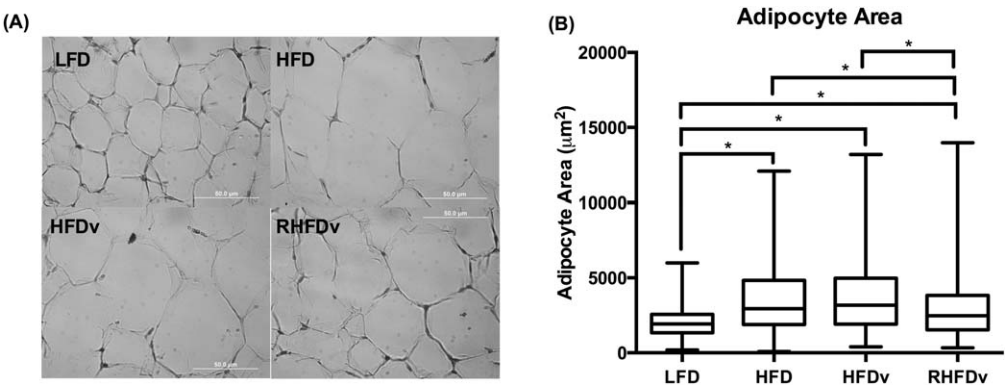

Figure 4 Adipocyte hypertrophy. (**A**) Representative histological sections of gonadal fat pads (400 × magnification) stained with hematoxylin and eosin to detect adipocyte boundaries. (**B**) Compared with LFD mice, increased adipocyte area caused by a high-fat diet in HFD, HFDv, and RHFDv mice. The median adipocyte area significantly decreased in RHFDv mice, but not in HFDv mice, compared with HFD mice. The data set was not normally distributed and is presented as the median, interquartile range, and minimum and maximum. *$P < 0.05$.

Effect of high-fat diet and LIV on abdominal adiposity

At the end of phase one, high-fat diet led to increased TAT, SAT, and VAT in HFD, HFDv, and RHFDv mice, as compared with LFD mice ($P < 0.05$, Figure 3B). During phase two, HFD, HFDv, and RHFDv mice showed continued increases in TAT (55%, 41%, and 43%, respectively, $P < 0.05$, Figure 3C). While SAT increased by 29% and 54%, VAT increased by 43% and 37% in HFDv and RHFDv mice, respectively, after 6 weeks of LIV intervention. HFD and HFDv mice showed significant increases in VAT (5,462% and 3,988%, respectively) during phase two, as compared with LFD mice ($P < 0.05$). Although not significantly different from HFD or HFDv mice, RHFDv mice showed a mitigated increase in VAT (3,458%, compared with LFD mice, $P =$ not significant) during phase two, demonstrating a prevention in VAT gain with 2 × 15 LIV.

Adipocyte hypertrophy in obesity mitigated by 2 × 15 LIV

Representative sections of adipocytes from gonadal adipose tissue are shown in Figure 4A. Whereas the median adipocyte area of LFD mice was 1,926 μm^2, median adipocyte areas in HFD and HFDv mice increased to 2,944 μm^2 and 3,177 μm^2, respectively ($P < 0.05$, Figure 4B). Although still significantly higher than in LFD mice, the median adipocyte area of RHFDv mice (2,478 μm^2) was reduced by 15% ($P < 0.05$) and 22% ($P < 0.05$), as compared with HFD and HFDv mice, respectively.

Obesity increases immune cell infiltration and inflammation in adipose tissue

Whereas B cell populations in HFD and HFDv mice increased by 203% and 240%, respectively ($P < 0.05$), the increase was limited to 155% in RHFDv mice ($P =$ not significant), as compared with LFD mice (Figure 5A). Similarly, $CD4^+$ T cell populations in HFD, HFDv, and RHFDv mice increased by 150% ($P < 0.05$), 132% ($P < 0.05$), and 94% ($P =$ not significant), respectively, as compared with LFD mice (Figure 5B). Following the same trend, macrophage populations in HFD, HFDv, and RHFDv mice increased by 137% ($P < 0.05$), 152% ($P < 0.05$), and 108% ($P =$ not significant), respectively, as compared with LFD mice ($n = 7$ for LFD mice, one data point excluded as an outlier) (Figure 5C). TNF-α gene expression in gonadal adipose tissue increased in HFD mice ($n = 7$ in HFD, one data point excluded as an outlier) and HFDv mice by 108% ($P < 0.05$) and 67% ($P < 0.05$), respectively, whereas it increased by 53% ($P =$ not significant) in RHFDv mice, as compared with LFD mice (Figure 5D).

Depleted percentage of MSCs in adipose tissue during obesity is partially restored with 2 × 15 LIV

MSCs in gonadal adipose tissue were quantified via flow cytometric analysis, as shown in Figure 6A. The percentage of MSCs (MSC%) compared with live cells in adipose tissue was lower in HFD, HFDv, and RHFDv mice by 55%, 43%, and 33%, respectively, than it was in LFD mice ($P < 0.05$). The MSC% in RHFDv mice (50%, $P < 0.05$), but not in HFDv mice (28%, $P =$ not significant), was significantly elevated as compared with HFD mice (Figure 6B). In addition, the MSC% exhibited a negative correlation with adipose tissue expression of TNF-α ($r = -0.48$, $P < 0.05$) (Figure 6C).

Obesity-induced glucose intolerance mitigated by 2 × 15 LIV

Fasting blood glucose was similar in all groups. Although not significantly different, the peak blood glucose, observed at 15 minutes after the intraperitoneal injection of dextrose, was elevated in HFD, HFDv, and RHFDv mice, as compared with LFD mice (Figure 7A). While blood glucose levels in HFD and HFDv mice remained elevated until 90 minutes after the glucose injection, as compared with LFD mice, RHFDv mice had returned to baseline by this time. Glucose intolerance was elevated by 15% in both HFD and HFDv mice ($P < 0.05$), whereas the increase was limited to 5% in RHFDv mice ($P =$ not significant), as compared with LFD mice (Figure 7B).

Insulin resistance during obesity improved by 2 × 15 LIV

As shown in Figure 7C, while high-fat diet feeding resulted in hyperinsulinemia in HFD and HFDv mice, as compared with LFD

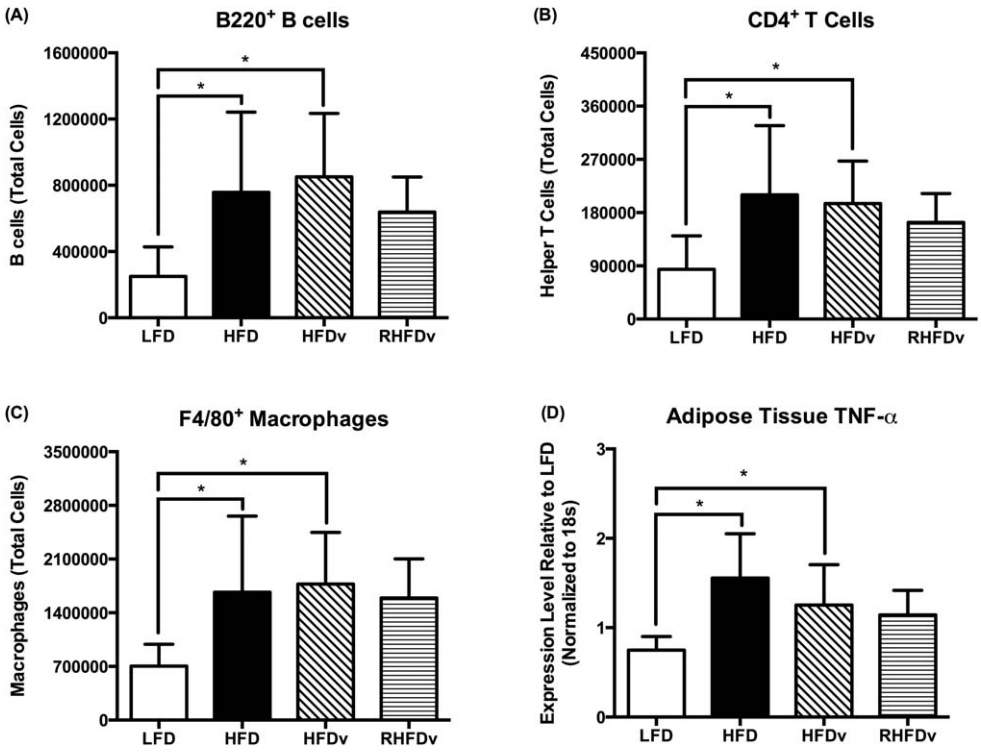

Figure 5 Adipose tissue inflammation. Significantly increased infiltration of (**A**) B220$^+$ B cells, (**B**) CD4$^+$ T cells, and (**C**) F4/80$^+$ macrophages in the gonadal adipose tissue of HFD and HFDv mice, but not RHFDv mice, compared with LFD mice. (**D**) Significantly increased gene expression of TNF-α, a proinflammatory cytokine, in the gonadal adipose tissue of HFD and HFDv mice, but not RHFDv mice, compared with LFD mice. All data sets were normally distributed, and data are presented as mean ± SD. *$P < 0.05$.

mice (238% and 189% higher fasting plasma insulin, respectively, $P < 0.05$), RHFDv attenuated hyperinsulinemia (126% higher fasting plasma insulin as compared with LFD, P = not significant). Adipose tissue gene expression of IRS1, a key player in insulin signaling, was reduced by 30% in HFD mice, as compared with LFD mice ($P < 0.05$). IRS1 expression significantly increased in RHFDv mice (31%, $P < 0.05$), but not in HFDv mice (2%, P = not significant), as compared with HFD mice (Figure 7D).

Discussion

Current treatments for obesity and related comorbidities in the form of lifestyle, pharmacological, and/or surgical interventions demonstrate limited success because of poor compliance, ineffectiveness, complications, morbidity, and/or mortality (30,31). In this study, we investigated the ability of LMMS, as an alternative to exercise, to suppress obesity-induced adipose tissue dysfunction and its sequelae, such as impaired glucose metabolism, in mice. Adult mice were chosen to better represent the pathogenesis observed in the majority of patients diagnosed with obesity (1). Here, we demonstrate that 2×15 LIV, but not 1×30 LIV, successfully mitigates obesity-induced adipose tissue dysfunction and its sequelae in adult mice.

There are a few limitations associated with this study. Control mice were switched from normal chow (13% of kilocalories from fat) to a low-fat diet (10% of kilocalories from fat) before beginning the study, which might have limited their adiposity gain more than if they were treated as age-matched controls. However, the low- and high-fat diet used here enabled us to keep the calories consumed from protein consistent between groups, giving a better comparison for the effects of fat consumption. In addition, we evaluated gonadal adipose tissue, as a representative for a VAT depot, throughout the study, and we do acknowledge that there may have been site-specific physiological and functional differences in other VAT and SAT depots; future studies can be done to evaluate these differences. Data interpretation of the impact of 2×15 LIV was limited to not having a significant difference between LFD and RHFDv mice, rather than to not having a significant difference between HFD and RHFDv mice (with the exception of adipocyte hypertrophy, MSC% in adipose tissue, and IRS1 expression in adipose tissue).

Evaluating gross changes in body habitus, 2 weeks of high-fat diet induced the obesity phenotype, as quantified by increased body weight and abdominal adiposity, before starting the LMMS treatment. All mice on high-fat diet, including those subjected to LMMS, continued to gain body weight and abdominal adiposity throughout the experiment, reaffirming the results of previous studies (9,10,14). Progression in weight gain was slowed by incorporating a refractory period between loading bouts (RHFDv), limiting the weight gain to 5% over the 6 weeks of phase two, as compared with the 11% in HFD mice and the 9% in HFDv mice acquired over the same period. Interestingly, despite continued increases in TAT, the distribution of abdominal adipose tissue in RHFDv mice shifted in

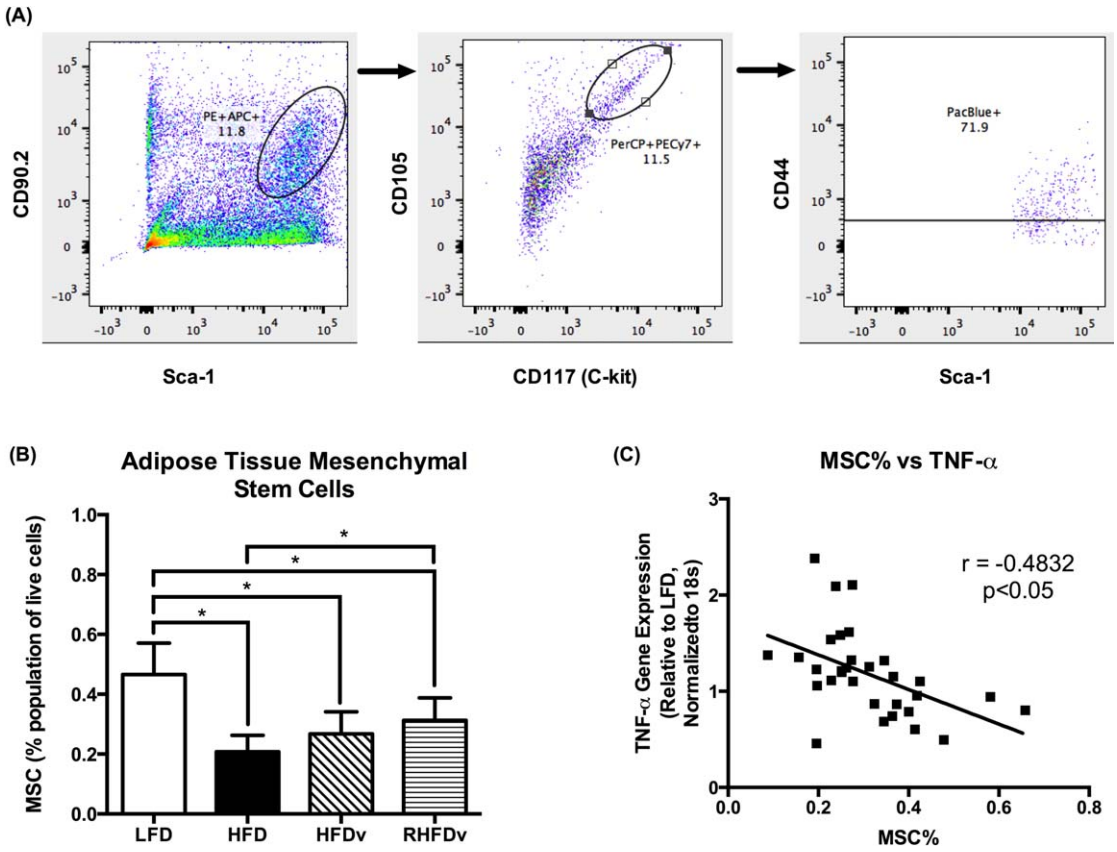

Figure 6 Adipose tissue MSCs and inflammation. (**A**) Representative gating scheme to determine MSC population (Sca-1^+CD90.2^+CD117^+CD105^+CD44^+) in adipose tissue. (**B**) Decreased adipose tissue MSC% in HFD, HFDv, and RHFDv mice, compared with LFD mice. The MSC% was rescued in RHFDv mice, but not in HFDv mice, compared with HFD mice. (**C**) Negative correlation between adipose tissue MSC% and adipose tissue TNF-α expression ($r = -0.4832$, $P < 0.05$). All data sets were normally distributed, and data are presented as mean ± SD. *$P < 0.05$. [Color figure can be viewed at wileyonlinelibrary.com]

comparison to that of HFD and HFDv mice, with the gain in RHFDv mice being a result of an increase in SAT. The gain in HFD and HFDv mice, however, was a result of an increase in VAT. Under normal physiological conditions, SAT is capable of creating new adipocytes to store excess energy intake, a function that gets impaired during obesity (32). We hypothesize that 2 × 15 LIV promotes adipogenesis in SAT, increasing its storage capability, to avoid fat accumulation in the viscera. Increased visceral adiposity has been associated with an increased likelihood of cardiovascular diseases, impaired glucose metabolism, and development of insulin resistance and has been shown overall to be a better predictor of mortality than subcutaneous adiposity (33). Hence, fat redistribution with 2 × 15 LIV, toward SAT and away from VAT, suggests a shift to a healthier body habitus.

Following changes in adipose tissue distribution, obesity also led to adipocyte hypertrophy in gonadal fat tissue, paralleled with increased infiltration of B cells, $CD4^+$ T cells, and macrophages within the tissue, as quantified by flow cytometry. Whereas B cells and $CD4^+$ T cells play a role in adaptive immunity (34), macrophages are known to secrete TNF-α, a proinflammatory cytokine (35). Here, we show an elevated gene expression for TNF-α in the adipose tissue from mice with obesity, as compared with LFD mice. The 2 × 15, but not 1 × 30, LIV resulted in significant suppression of adipocyte hypertrophy and a concomitant reduction in immune cell infiltration in adipose tissue, leading to reduced expression of TNF-α in adipose tissue. Because MSCs have been shown to play a role in immunomodulation and immunosuppression (12,13), we further quantified the MSC population in gonadal adipose tissue. Whereas adipose tissue MSC populations decreased with obesity, they were significantly restored with 2 × 15 LIV. It is still unclear what causes the increase in adipose tissue MSCs with 2 × 15 LIV. Some of the possible causes could be increased proliferation of existing adipose tissue MSCs, decreased differentiation of adipose tissue MSCs into adipocytes, or increased migration of bone marrow MSCs into adipose tissue (10,19,36). We also observed a significant negative correlation between MSCs and inflammation in adipose tissue, indicating an association between the variables; as MSCs in adipose tissue increase, inflammation in the tissue decreases. Although the relationship is not causative as shown, future studies can define the role of MSCs in immunosuppression more accurately to serve as a unique strategy for combating obesity-associated adipose tissue dysfunction.

High-fat diet resulted in impaired glucose metabolism, a sequela of adipose tissue dysfunction. HFD mice had significantly higher glucose intolerance than LFD mice, and this intolerance was successfully mitigated by 2 × 15 LIV, but not by 1 × 30 LIV. Interestingly, the

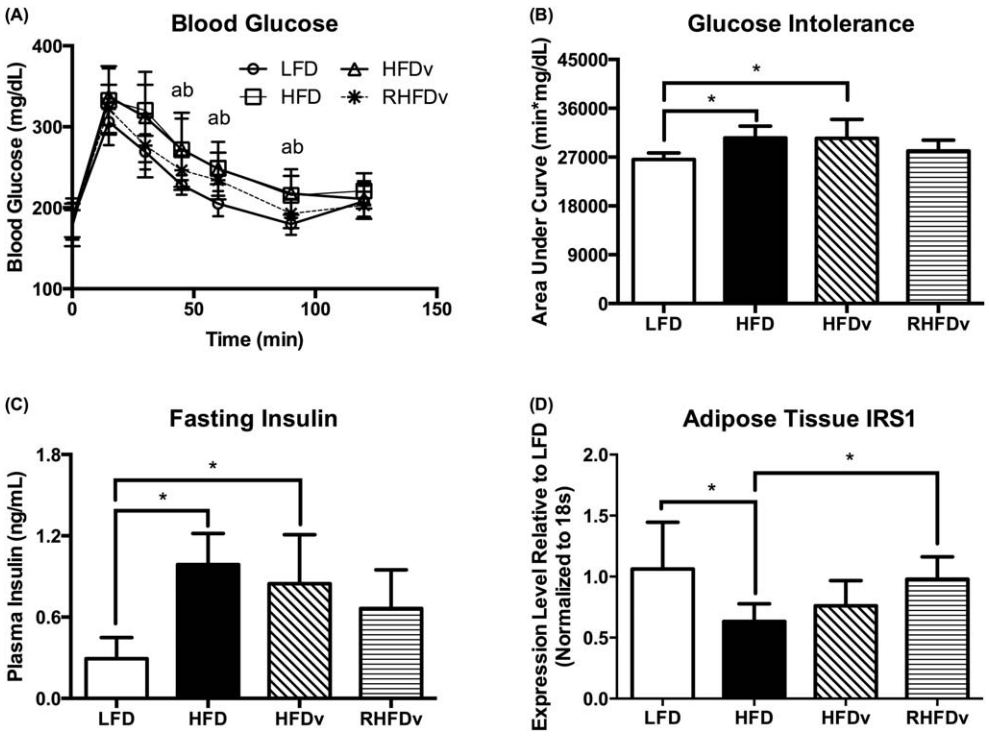

Figure 7 Glucose intolerance as a sequelae of adipose tissue dysfunction. (**A**) Change in blood glucose for 2 hours after intraperitoneal dextrose injection. There was an improved blood glucose elimination in RHFDv mice, compared with HFD and HFDv mice. (**B**) Increased glucose intolerance in HFD and HFDv mice, but not in RHFDv mice, compared with LFD mice, as measured by the area under the blood glucose curve in Figure 7A. (**C**) Increased fasting insulin in HFD and HFDv mice, but not in RHFDv mice, compared with LFD mice. (**D**) Compared with LFD mice, reduced expression of IRS1, an insulin receptor, in the adipose tissue of HFD mice. The elevated expression of IRS1 in RHFDv mice as compared with HFD mice, despite high-fat diet, is shown. All data sets were normally distributed, and data are presented as mean ± SD. $^{a}P < 0.05$, LFD versus HFD. $^{b}P < 0.05$, LFD versus HFDv. $^{*}P < 0.05$.

impaired glucose tolerance in HFD and HFDv mice was a result of insulin resistance, as was evident by the hyperinsulinemia and reduced expression of IRS1 in gonadal fat. IRS1 is an important player in the insulin-signaling pathway, which can drive inactivation of phosphoinositide 3-kinase, leading to hyperglycemia, hyperinsulinemia, and insulin resistance (37). Alternatively, RHFDv mice showed mitigated hyperinsulinemia and an increased expression of IRS1 in gonadal fat as compared with HFD mice, indicating reduced insulin resistance. The effectiveness of 2×15 LIV, but not of 1×30 LIV, in improving glucose metabolism contradicts the results of the previous study, in which one bout of 20-minute vibration per day showed improved glucose metabolism (38). However, this previous study utilized young mice, reaffirming that the mechanosensitivity might indeed be age dependent and that the inclusion of a refractory period in LMMS can boost the declined mechanosensitivity.

The beneficial effect of 2×15 LIV, but not 1×30 LIV, in rescuing obesity-induced adipose tissue dysfunction and impaired glucose metabolism in adults suggests that the scheduling of LMMS is of more importance than the total duration. This result reinforces the outcomes from previous studies, which have demonstrated an enhanced response toward mechanical stimulation or an exercise regime with incorporation of either a refractory period between bouts or a rest period between individual loading cycles (18,19,39). A previous *in vitro* study demonstrated that MSCs respond to LMMS through coupling of the cytoskeleton and nucleus and that the first bout of LMMS leads to perinuclear cytoskeletal remodeling in the form of increased focal adhesions and increased RhoA activity, leading to an amplified mechanical response to the second bout of LMMS (40). Salutary effects of 2×15 LIV can then be partially attributed to cytoskeletal reorganization of mechanosensitive cells, such as MSCs, *in vivo*.

Conclusion

Overall, this study demonstrates the body habitus changes consistent with obesity, such as increased adiposity within the visceral cavity and increased adipocyte size. The consequently elevated adipose tissue inflammation may contribute to increased insulin resistance and glucose intolerance. Although a single bout of LMMS was not successful in reducing adipose tissue dysfunction and sequelae caused by chronic obesity, incorporating a 5-hour refractory period between two bouts of LMMS reduced visceral adiposity, adipocyte size, and adipose tissue inflammation and increased the MSC population in the adipose tissue, resulting in improved insulin sensitivity and glucose metabolism. These data may provide insight into the means by which exercise provides salutary signals to those struggling with obesity and imports that the scheduling of the physical activity may be as critical as the activity itself. And although LIV can only be

viewed as a surrogate for exercise, it does provide a means of delivering a signal that mitigates some of the complications of obesity, while not requiring strenuous exertion. O

Acknowledgments

The authors are grateful for the technical assistance provided by Alyssa Tuthill, Divya Krishnamoorthy, Tee Pamon, Jeyantt Sankaran, Shabab Hussain, and Ariel Yang.

References

1. Ogden CL, Carroll MD, Kit BK, Flegal KM. Prevalence of childhood and adult obesity in the United States, 2011-2012. *JAMA* 2014;311:806-814.
2. Finkelstein EA, Trogdon JG, Cohen JW, Dietz W. Annual medical spending attributable to obesity: payer-and service-specific estimates. *Health Aff (Millwood)* 2009;28:w822-w831.
3. Fantuzzi G. Adipose tissue, adipokines, and inflammation. *J Allergy Clin Immunol* 2005;115:911-919;quiz 920.
4. Ghigliotti G, Barisione C, Garibaldi S, et al. Adipose tissue immune response: novel triggers and consequences for chronic inflammatory conditions. *Inflammation* 2014;37:1337-1353.
5. Qatanani M, Lazar MA. Mechanisms of obesity-associated insulin resistance: many choices on the menu. *Genes Dev* 2007;21:1443-1455.
6. Vieira VJ, Valentine RJ, Wilund KR, Antao N, Baynard T, Woods JA. Effects of exercise and low-fat diet on adipose tissue inflammation and metabolic complications in obese mice. *Am J Physiol Endocrinol Metab* 2009;296:E1164-E1171.
7. Kawanishi N, Mizokami T, Yano H, Suzuki K. Exercise attenuates m1 macrophages and cd8 + t cells in the adipose tissue of obese mice. *Med Sci Sports Exerc* 2013;45:1684-1693.
8. Villareal DT, Chode S, Parimi N, et al. Weight loss, exercise, or both and physical function in obese older adults. *N Engl J Med* 2011;364:1218-1229.
9. Luu YK, Capilla E, Rosen CJ, et al. Mechanical stimulation of mesenchymal stem cell proliferation and differentiation promotes osteogenesis while preventing dietary-induced obesity. *J Bone Miner Res* 2009;24:50-61.
10. Luu YK, Pessin JE, Judex S, Rubin J, Rubin CT. Mechanical signals as a non-invasive means to influence mesenchymal stem cell fate, promoting bone and suppressing the fat phenotype. *Bonekey Osteovision* 2009;6:132-149.
11. Rubin CT, Capilla E, Luu YK, et al. Adipogenesis is inhibited by brief, daily exposure to high-frequency, extremely low-magnitude mechanical signals. *Proc Natl Acad Sci U S A* 2007;104:17879-17884.
12. Bartholomew A, Sturgeon C, Siatskas M, et al. Mesenchymal stem cells suppress lymphocyte proliferation in vitro and prolong skin graft survival in vivo. *Exp Hematol* 2002;30:42-48.
13. Nemeth K, Leelahavanichkul A, Yuen PS, et al. Bone marrow stromal cells attenuate sepsis via prostaglandin e(2)-dependent reprogramming of host macrophages to increase their interleukin-10 production. *Nat Med* 2009;15:42-49.
14. Chan ME, Adler BJ, Green DE, Rubin CT. Bone structure and B-cell populations, crippled by obesity, are partially rescued by brief daily exposure to low-magnitude mechanical signals. *FASEB J* 2012;26:4855-4863.
15. Klein-Nulend J, Sterck JG, Semeins CM, et al. Donor age and mechanosensitivity of human bone cells. *Osteoporos Int* 2002;13:137-146.
16. Gilsanz V, Wren TA, Sanchez M, Dorey F, Judex S, Rubin C. Low-level, high-frequency mechanical signals enhance musculoskeletal development of young women with low bmd. *J Bone Miner Res* 2006;21:1464-1474.
17. Uzer G, Fuchs RK, Rubin J, Thompson WR. Concise review: plasma and nuclear membranes convey mechanical information to regulate mesenchymal stem cell lineage. *Stem Cells* 2016;34:1455-1463.
18. Robling AG, Burr DB, Turner CH. Recovery periods restore mechanosensitivity to dynamically loaded bone. *J Exp Biol* 2001;204:3389-3399.
19. Sen B, Xie Z, Case N, Styner M, Rubin CT, Rubin J. Mechanical signal influence on mesenchymal stem cell fate is enhanced by incorporation of refractory periods into the loading regimen. *J Biomech* 2011;44:593-599.
20. Sen B, Guilluy C, Xie Z, et al. Mechanically induced focal adhesion assembly amplifies anti-adipogenic pathways in mesenchymal stem cells. *Stem Cells* 2011;29:1829-1836.
21. Appiah-Nkansah K. Integration of refractory periods in the administration of low-magnitude mechanical signals increases mesenchymal stem cell numbers in the bone marrow. Stony Brook University, 2011, Master of Science:25-27. https://ir.stonybrook.edu/jspui/handle/11401/71558
22. Judex S, Luu YK, Ozcivici E, Adler B, Lublinsky S, Rubin CT. Quantification of adiposity in small rodents using micro-ct. *Methods* 2010;50:14-19.
23. Luu YK, Lublinsky S, Ozcivici E, et al. In vivo quantification of subcutaneous and visceral adiposity by micro-computed tomography in a small animal model. *Med Eng Phys* 2009;31:34-41.
24. Luu YK, Ozcivici E, Capilla E, et al. Development of diet-induced fatty liver disease in the aging mouse is suppressed by brief daily exposure to low-magnitude mechanical signals. *Int J Obes (Lond)* 2010;34:401-405.
25. Blazquez-Martinez A, Chiesa M, Arnalich F, Fernandez-Delgado J, Nistal M, De Miguel MP. C-kit identifies a subpopulation of mesenchymal stem cells in adipose tissue with higher telomerase expression and differentiation potential. *Differentiation* 2014;87:147-160.
26. Ying W, Tseng A, Chang RC, et al. Mir-150 regulates obesity-associated insulin resistance by controlling b cell functions. *Sci Rep* 2016;6:20176. doi:10.1038/srep20176
27. Deng T, Lyon CJ, Minze LJ, et al. Class II major histocompatibility complex plays an essential role in obesity-induced adipose inflammation. *Cell Metab* 2013;17:411-422.
28. Weisberg SP, McCann D, Desai M, Rosenbaum M, Leibel RL, Ferrante AW, Jr. Obesity is associated with macrophage accumulation in adipose tissue. *J Clin Invest* 2003;112:1796-1808.
29. Zhang J, Tang H, Zhang Y, et al. Identification of suitable reference genes for quantitative RT-PCR during 3T3-L1 adipocyte differentiation. *Int J Mol Med* 2014;33:1209-1218.
30. Foreyt JP, Poston WS, 2nd. The challenge of diet, exercise and lifestyle modification in the management of the obese diabetic patient. *Int J Obes Relat Metab Disord* 1999;23(suppl 7):S5-S11.
31. Peckmezian T, Hay P. A systematic review and narrative synthesis of interventions for uncomplicated obesity: weight loss, well-being and impact on eating disorders. *J Eat Disord* 2017;5:15. doi:10.1186/s40337-017-0143-5
32. Gustafson B, Hammarstedt A, Hedjazifar S, Smith U. Restricted adipogenesis in hypertrophic obesity: the role of WISP2, WNT, and BMP4. *Diabetes* 2013;62:2997-3004.
33. Ritchie SA, Connell JM. The link between abdominal obesity, metabolic syndrome and cardiovascular disease. *Nutr Metab Cardiovasc Dis* 2007;17:319-326.
34. Travers RL, Motta AC, Betts JA, Bouloumie A, Thompson D. The impact of adiposity on adipose tissue-resident lymphocyte activation in humans. *Int J Obes (Lond)* 2015;39:762-769.
35. Unoki H, Bujo H, Jiang M, Kawamura T, Murakami K, Saito Y. Macrophages regulate tumor necrosis factor-alpha expression in adipocytes through the secretion of matrix metalloproteinase-3. *Int J Obes (Lond)* 2008;32:902-911.
36. Uzer G, Pongkitwitoon S, Chan ME, Judex S. Vibration induced osteogenic commitment of mesenchymal stem cells is enhanced by cytoskeletal remodeling but not fluid shear. *J Biomech* 2013;46:2296-2302.
37. Guo S. Insulin signaling, resistance, and the metabolic syndrome: insights from mouse models into disease mechanisms. *J Endocrinol* 2014;220:T1-T23.
38. McGee-Lawrence ME, Wenger KH, Misra S, et al. Whole-body vibration mimics the metabolic effects of exercise in male leptin receptor deficient mice [published online March 15, 2017]. *Endocrinology* 2017;158:1160-1171.
39. Srinivasan S, Weimer DA, Agans SC, Bain SD, Gross TS. Low-magnitude mechanical loading becomes osteogenic when rest is inserted between each load cycle. *J Bone Miner Res* 2002;17:1613-1620.
40. Uzer G, Thompson WR, Sen B, et al. Cell mechanosensitivity to extremely low-magnitude signals is enabled by a linced nucleus. *Stem Cells* 2015;33:2063-2076.